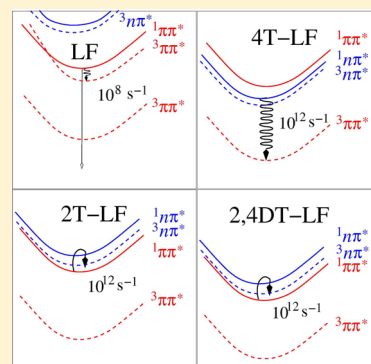


Photophysics of Flavin Derivatives Absorbing in the Blue-Green Region: Thioflavins As Potential Cofactors of Photoswitches

Christel M. Marian,^{*,†} Setsuko Nakagawa,[‡] Vidisha Rai-Constapel,[§] Bora Karasulu,^{||} and Walter Thiel^{||}[†]Institute of Theoretical and Computational Chemistry, Heinrich Heine University Düsseldorf, Universitätsstr. 1, D-40225 Düsseldorf, Germany[‡]Department of Human Life and Environment, Kinjo Gakuin University, Nagoya 463 8521, Japan[§]Institute of Theoretical and Computational Chemistry, Heinrich Heine University Düsseldorf, Universitätsstr. 1, D-40225 Düsseldorf, Germany^{||}Max-Planck-Institut für Kohlenforschung, Kaiser-Wilhelm-Platz 1, 45470 Mülheim an der Ruhr, Germany

S Supporting Information

ABSTRACT: The purpose of this study was to find flavin derivatives with absorption maxima in the blue-green region of the visible spectrum that might be used as alternative cofactors in blue-light photoreceptors. To this end, the vertical absorption spectra of eight lumiflavin-related compounds were calculated by means of quantum chemical methods. The compounds differ from lumiflavin by the substitution of an S atom for an O atom at the 2- and/or 4-positions of the isoalloxazine core, the substitution of an N atom for a CH group in the 6- and/or 9-positions, or an extension of the π system at the 7- and 8-positions. For the three most promising compounds, 2-thio-lumiflavin, 4-thio-lumiflavin, and 2,4-dithio-lumiflavin, the quantum chemical investigations were extended to include geometry relaxations in the excited states, rates for spin-forbidden transitions and an estimate of spectral shifts brought about by polar protic environments. We find these thiocarbonyl compounds to have very promising excited-state properties. They absorb in the blue-green wavelength regime around 500 nm, i.e., substantially red-shifted with respect to lumiflavin that is the cofactor of natural blue-light photoreceptors. Their triplet quantum yields are predicted to be close to unity while their triplet lifetimes are long enough to enable bimolecular photochemical reactions. The combination of these properties makes the thioflavins potentially suitable candidates as cofactors in biomimetic photoswitches.



■ INTRODUCTION

Recent years have seen a boost of studies on flavin photochemistry and physics especially due to their decisive role in blue light-mediated signal transduction in bacteria, archaea, plants and fungi.^{1–5} Light, oxygen, and voltage-sensitive (LOV) domains are protein photosensors that bind a flavin mononucleotide (FMN) cofactor (Figure 1) non-covalently. Upon absorption of blue light, the LOV domain undergoes a photocycle. The primary step after light absorption

hereby involves a rapid decay of the excited singlet state to the lowest excited triplet state via an intersystem crossing (ISC) mechanism. In a second step a metastable covalent adduct of a nearby cysteine residue and the isoalloxazine framework of the chromophore is generated resulting in a structural signal that is transduced to an effector domain.

LOV domains can be fused to cellular effector proteins to create artificial light-sensitive variants enabling photochemical regulation of protein function.^{5–8} A genetically encoded photoactivatable Rac fused to a LOV domain from phototropin has even been used to control the motility of living cells.⁹ In some applications, however, there is a need for red-shifted photochemical tools with enhanced light-sensitivity.¹⁰ It could thus be interesting to replace the cofactor of natural blue-light receptors by a flavin derivative with reduced photoexcitation energy (thereby minimizing the radiation damage of the surrounding biological material) while keeping the photocycle intact.

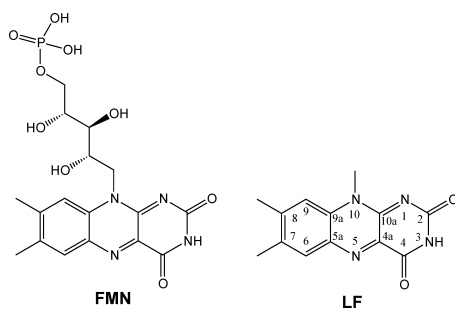


Figure 1. Chemical structures of flavin mononucleotide (FMN) and lumiflavin (LF) with IUPAC atomic labels.

Received: October 2, 2013

Revised: January 29, 2014

Published: January 30, 2014

Riboflavin-5'-phosphate, also known as FMN (Figure 1), can be divided into two parts: the isoalloxazine (benzo[*g*]pteridine-2,4(3H,10H)-dione) core ring that is the blue-light sensitive part and the ribophosphyl chain that is required for the signal transduction. In lumiflavin (LF) the ribophosphyl chain of FMN in 10-position has been replaced for a methyl group. Since the photophysical and photochemical behavior of flavins is dominated by the isoalloxazine core, experimental absorption and emission spectra of FMN and LF are very similar. In contrast, electronic modification of the isoalloxazine core, such as the substitution of a CH group for the nitrogen atom in 1- or 5-positions, does not only influence the absorption characteristics, but has also strong impact on the triplet formation and the photocycle in LOV domains.^{11–14}

In this work, the photophysics of eight LF-related compounds (Figure 2) has been investigated. The idea was

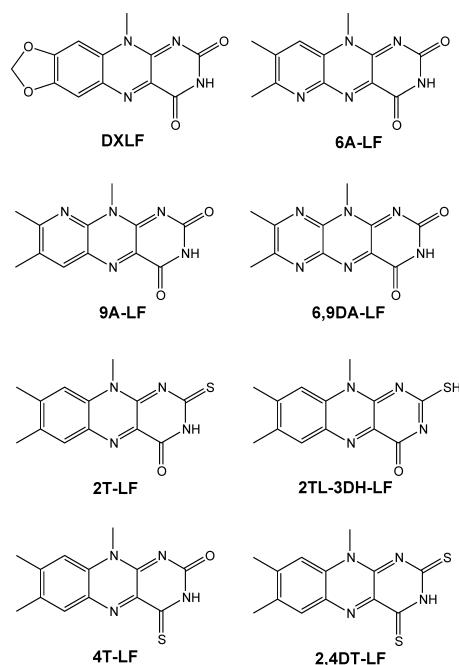


Figure 2. Chemical structures of flavin derivatives studied in this work.

to modify the π system by either replacing species in the isoalloxazine core by isovalent atoms or by exchanging substituents for more extended ones. In doing so, electrostatic properties and spatial limitations in the LOV pocket have been taken into consideration. The methyl groups attached to the 7- and 8-positions of the native LF can, for instance, be replaced by a trifluoromethyl, mercapto, methoxy, or hydroxy group but not by very bulky substituents.^{15,16} At the hydrophilic side of the LOV pocket, the pteridine moiety is surrounded by several hydrogen bond donors and acceptors. It may thus be assumed that the hydrogen bond network plays an essential role in the photocycle. Here, we report calculations on a derivate in which a $-\text{O}-\text{CH}_2-\text{O}-$ bridge has been attached to the carbon atoms in 7- and 8-positions, respectively, thus forming a dioxolane ring (DXLF). Furthermore, we have substituted CH groups for N atoms in the benzene moiety of the isoalloxazine core (6A-LF, 9A-LF, and 6,9DA-LF). With regard to the pteridine moiety, we investigate the photophysical effects occurring when the carbonyl groups in 2- and/or 4-positions are replaced by thiocarbonyl groups (2T-LF, 4T-LF, and 2,4DT-LF). In

addition, an iminothiol tautomer of 2T-LF, 2TL-3DH-LF, has been studied.

The most promising compounds, i.e., the thiolumiflavins, have been investigated in more detail. The first absorption bands of 2-thio-lumiflavin (2T-LF) and 4-thio-lumiflavin (4T-LF) are known to be red-shifted with respect to LF.¹⁷ In contrast, the location of the dark states ($n\pi^*$ states, triplet $\pi\pi^*$ states) that are crucial for the photophysics and photochemistry of the compounds are widely unknown. Starting with the isolated chromophores, the impact of solvent effects on the excited-state properties is evaluated. ISC and phosphorescence rate constants are determined to judge both the accessibility and the lifetime of the T_1 state that is supposed to be the photochemically active state in LOV domains of biological blue-light photoreceptors. Our results will be compared to corresponding data for LF that has been the subject of recent studies in our group.^{11,18,19}

METHODS AND COMPUTATIONAL DETAILS

Geometry optimizations of the ground state and the lowest triplet states were carried out at the level of (unrestricted) density functional theory ((U)DFT) using the Turbomole 6.3²⁰ program package. For all calculations, we employed the standard TZVP basis set from the Turbomole library.²¹ The B3LYP functional^{22,23} was used for optimizing the molecular geometries. Unless otherwise noted C_s symmetry constraints were imposed on the ground and excited state geometries of the isolated chromophores. Electronically excited singlet and triplet state geometries were determined at the level of time-dependent DFT²⁴ (TDDFT).²⁵ To ensure that the resulting geometries correspond to true minima of the potential energy hypersurface (PEH), harmonic vibrational frequencies were calculated numerically with the program SNF.²⁶

Vertical electronic excitation energies and dipole moments were obtained from subsequent single-point calculations using the combined density functional theory/multireference configuration interaction (DFT/MRCI) method of Grimme and Waletzke.²⁷ In this method, the MRCI expansion is built up in a one-particle basis of Kohn–Sham orbitals employing the B3LYP functional^{28,29} and matrix elements are scaled using empirically determined parameters. Typically, this method yields excitation energies with errors below 0.2 eV.^{27,30} Technical details of the DFT/MRCI calculations were chosen to be identical to those in the original work of Salzmann et al. on LF.¹⁸

ISC rate constants have been determined perturbationally, making use of the Fermi golden rule ansatz. In this ansatz, the decay rate of an initially populated $\Psi_{S_a, \nu_{aj}}$ vibronic state via ISC to a quasicontinuum of final vibronic states $\Psi_{T_b, \nu_{bk}}^\alpha$ is given by

$$k_{\text{ISC}} = \frac{2\pi}{\hbar} \sum_{\alpha} \sum_k |\langle \Psi_{S_a, \nu_{aj}} | \hat{H}_{\text{SO}} | \Psi_{T_b, \nu_{bk}}^\alpha \rangle|^2 \delta(E_{aj} - E_{bk}) \quad (1)$$

Typically, eq 1 is expanded into a Taylor series around an appropriately chosen reference point q_0 , e.g., the equilibrium geometry of the initial state. Furthermore, the Condon approximation

$$k_{\text{ISC}}^{\text{FC}} \approx \frac{2\pi}{\hbar} \sum_{\alpha} |\langle \Psi_{S_a} | \hat{H}_{\text{SO}} | \Psi_{T_b}^\alpha \rangle_{q_0}|^2 \sum_k |\langle \nu_{aj} | \nu_{bk} \rangle|^2 \delta(E_{aj} - E_{bk}) \quad (2)$$

has been employed, i.e., it is assumed that the coupling between the initial and the final states can be separated into an electronic and a vibrational factor. This assumption is usually fulfilled in good approximation for El-Sayed allowed ISC, e.g., $^1n\pi^* \rightarrow ^3\pi\pi^*$ and $^1\pi\pi^* \rightarrow ^3n\pi^*$. Electronic spin–orbit matrix elements (SOMEs) between the DFT/MRCI wave functions in eq 2 have been computed using the spin–orbit coupling kit (Spock).^{31,32} For reasons of efficiency, the one-center mean-field approximation to the Breit–Pauli Hamiltonian has been used for the description of the spin–orbit coupling.^{33,34} It has been shown that the accuracy of this approximation lies within better than 5% of the full treatment.^{35,36} The vibrational contributions to the rate in eq 2 have been determined using a time-dependent approach.³⁷ Briefly, a Fourier transform representation of delta function appearing in eq 2 is employed.

$$\delta(E_{aj} - E_{bk}) = \int_{-\infty}^{+\infty} e^{it(E_{aj} - E_{bk})} dt \quad (3)$$

In the harmonic oscillator model and making use of the Condon approximation, the ISC rate can then be determined by numerical integration of

$$k_{\text{ISC}}^{\text{corr}} = |\langle \Psi_S | \hat{H}_{\text{SO}} | \Psi_T \rangle|^2 \int_{-\infty}^{\infty} dt G(t) e^{it(\Delta E_{\text{ST}}^0 + \frac{1}{2} T_T \Omega_S)} \quad (4)$$

where $G(t)$ is a generating function

$$G(t) = 2^{N/2} \sqrt{\frac{\det(S^{-1} \Omega_S \Omega_T)}{\det(J^\dagger \Omega_T B J + \Omega_S) \det(J^\dagger \Omega_T B^{-1} J + \Omega_S)}} \exp(D^\dagger (\Omega_T B J (J^\dagger \Omega_T B J + \Omega_S)^{-1} J^\dagger \Omega_T B - \Omega_T B) D)$$

that contains diagonal matrices Ω_S , Ω_T , S , and B with elements $(\Omega_S)_{ii} = \omega_{S_i}$, $(\Omega_T)_{ii} = \omega_{T_i}$, $S_{ii} = \sinh(i\omega_{T_i} t)$, $B_{ii} = \tanh(i\omega_{T_i} t/2)$. Herein, ω_{S_i} and ω_{T_i} represent the harmonic vibrational frequencies of the initial and final states, respectively. The mass-weighted normal modes of the final state are related to their counterparts of the initial state by the Duschinsky transformation³⁸ $Q_T = JQ_S + D$ where J is the Duschinsky rotation matrix and D the displacement vector. The Fourier transform of a Gaussian function of width 10 cm^{-1} was used to damp the oscillations of the time-correlation function. For its numerical integration, we have chosen an interval of 12 ps and 2^{18} grid points. Despite the inherent approximations and the uncertainty of the terms entering eq 2, we consider the order of magnitude of the calculated rate constants to be reliable. For further details on the theory and the methods for calculating spin–orbit coupling and ISC see, for instance, a recent review article.³⁹

For second-order spin-forbidden properties, such as phosphorescence rates, the convergence of sum-over-state perturbation expressions is known to be very slow.⁴⁰ For this reason, we use the DFT/MRSOCI, a multireference spin–orbit configuration interaction program,⁴¹ to compute spin–orbit coupled DFT/MRCI wave functions for this purpose. Since we are interested only in the $T_1 \rightarrow S_0$ radiative transition, it is sufficient to determine the four lowest roots of the MRSOCI matrix. To avoid numerical inaccuracies, a tight convergence threshold of $10^{-8} E_h$ was imposed in the Davidson procedure of the DFT/MRSOCI step.

Dipole transition matrix elements and oscillator strengths were evaluated in their length forms at the DFT/MRCI (fluorescence) or DFT/MRSOCI (phosphorescence) levels.

To estimate spectral shifts due to electrostatic interaction in polar solvents we employed the conductor-like screening model (COSMO) which is implemented in the TURBOMOLE package.^{42,43} Relative permittivities of $\epsilon_r = 78$ (water), $\epsilon_r = 33$ (acetonitrile), and $\epsilon_r = 4$ were used. A value of $\epsilon_r = 4$ corresponds to a typical protein environment^{44,45} and is also close to the permittivity of chloroform $\epsilon_r \approx 4.8$ at room temperature. When COSMO was applied, the MRCI expansion was built up from the one-particle basis of COSMO optimized Kohn–Sham orbitals. Because of technical reasons, C_1 symmetry had to be used for all DFT/MRCI calculations involving COSMO. For both, singlet and triplet multiplicity, 20 roots were computed. Since COSMO cannot properly model hydrogen bonding, the effects of hydrogen bonding in aqueous solution were mimicked by microhydration. For this purpose, we placed four water molecules next to the hetero atoms of the isalloxazine ring and optimized the ground state without symmetry constraints. In a further approach, the two previous solvation models were combined.

RESULTS AND DISCUSSION

Vertical excitation spectra in vacuum of all compounds are collected in Tables S1 and S2 of the Supporting Information (SI). It is seen that the aza substitution in the benzene moiety of the isalloxazine ring does not alter the essential absorption characteristics with respect to LF. In all three cases, the first bright transition is found at 2.94–2.97 eV, i.e., these derivatives absorb at much too short wavelengths (417–422 nm) to be interesting in the present context. Even a red shift of 0.1–0.15 eV due to solvent–solute interaction in water, as may be expected from the native compound, will not place the absorption in these molecules to the desired wavelength regime. However, 6A-LF, 9A-LF, and 6,9DA-LF might be interesting from a different point of view: Their triplet $n\pi^*$ states are located at lower energy than in LF which in turn could help increasing the ISC rates in solution. For a detailed discussion of solvent effects on the intermediate triplet formation in flavins the reader is referred to former work.¹⁸

The absorption wavelength of the first band of DXLF is shifted into the desired direction. In the gas phase, we obtain a vertical excitation energy of 2.84 eV (436 nm) for the first $^1(\pi \rightarrow \pi^*)$ transition. Adiabatically the excitation energy is lowered to 2.60 eV, i.e., we expect the band origin to lie at 477 nm. Solvent effects stabilize the upper state slightly so that the band origin (488 nm) could fit into the required wavelength window. In this compound, we encounter a different problem, however. Its first triplet $n\pi^*$ state that is essential for a fast ISC mechanism employing either direct or vibronic spin–orbit coupling is energetically not easily accessible, neither in the gas phase nor in solution. The iminothiol tautomer of 2T-LF, 2TL-3DH-LF, exhibits a seemingly ideal first absorption band with origin at 511 nm (2.43 eV) and maximum at 462 nm (2.68 eV) in vacuum. These values change only marginally upon solvation in water, in very good agreement with experimental values measured for the corresponding methylthioether.¹⁷ However, Dudley et al. report this 2-methylthioether (and the corresponding 4-methylthioether) to be chemically instable. According to these authors, they are easily protonated in 1-position with subsequent fast hydrolysis to yield LF.¹⁷

On these grounds, only the spectra and the photophysics of the thionyl compounds are presented and discussed in more detail in the following. For comparison, results of native LF have been taken from the work of Salzmann et al.^{11,18}

2-Thio-lumiflavin. Vacuum. Geometry optimization of the electronic ground state yields a planar nuclear arrangement of the ring system. Bond lengths of the ground and excited state structures are shown in Table S3 of the SI. Besides the obvious fact that the $C_2=S$ bond is considerably longer than the corresponding $C_2=O$ bond (167 vs 121 pm), only slight changes of the geometry parameters are observed when comparing 2T-LF with LF. As a result of the weaker double bond character of the $C_2=S$ bond, the neighboring C_2-N_1 and C_2-N_3 bonds slightly contract with respect to LF. All other geometry parameters are nearly unchanged.

With regard to electronic structure, the introduction of the thionyl group in 2-position is found to have a pronounced effect. At the molecular orbital (MO) level, the highest occupied molecular orbital (HOMO) is a π orbital (π_H) that exhibits a large amplitude on the sulfur center (Figure 3)

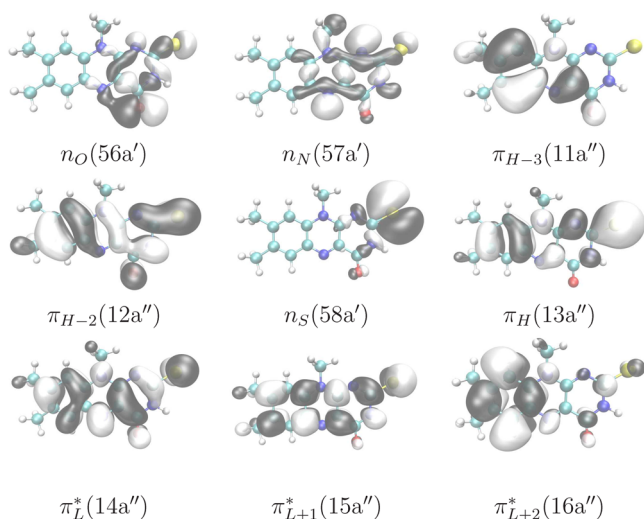


Figure 3. Frontier orbitals of 2T-LF at the optimized ground-state geometry. (Isovalue = 0.02.)

whereas the π system in the HOMO of LF is delocalized over the whole ring system (Figure 4 in ref 11). The corresponding π -MO of 2T-LF is only the third-highest occupied MO (π_{H-2}). The second-highest occupied MO of 2T-LF is mainly comprised of the nonbonding in-plane 3p orbital of sulfur (n_S). Other occupied MOs that are important for the characterization of the low-lying electronic states are the nonbonding in-plane orbital on oxygen (n_O) and a σ^* -type orbital with large contributions of in-plane p orbitals on the N_1 and N_3 atoms which we denote by n_N . The three lowest unoccupied molecular orbitals (LUMOs) are similar in shape and energetic order in 2T-LF and LF. While the LUMO (π_L^*) as well as the next higher MO (π_{L+1}^*) are delocalized over the ring system, π_{L+2}^* concentrates in the benzene ring. It is thus the antibonding counterpart of the π_{H-3} orbital.

The different shapes and energetic orders of the MOs in 2T-LF and LF are reflected in the electronic spectra. In Table 1, vertical absorption energies of 2T-LF are shown. In the singlet manifold, the lowest excited state corresponds to a $^1(n_S \rightarrow \pi_L^*)$ excitation with negligible oscillator strength. The strong first absorption (oscillator strength $f(r) \approx 0.51$) is associated with the second excited singlet state $^1(\pi_H \rightarrow \pi_L^*)$. In both cases, the transition is accompanied by an electron transfer from the sulfur region to the delocalized π system. Thus, the electric dipole moments of the two lowest-lying electronically excited

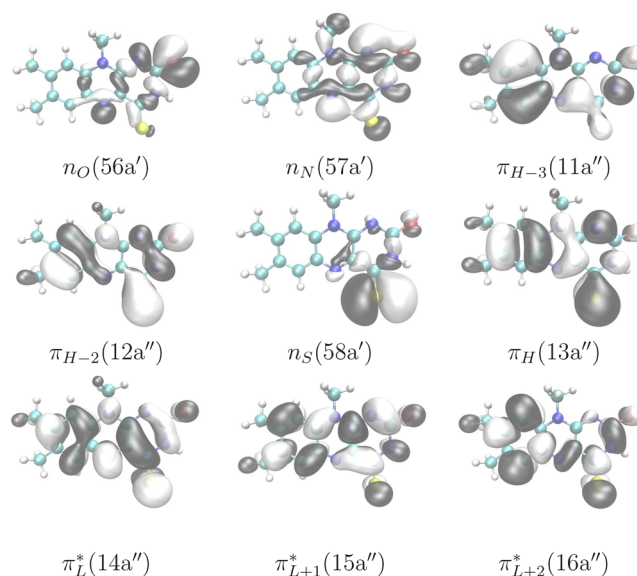


Figure 4. Frontier orbitals of 4T-LF at the optimized ground-state geometry. (Isovalue = 0.02.)

Table 1. Vertical Excitation Spectra of 2T-LF in the Gas Phase and in Water Solution

state	electronic structure	gas phase		water solution		
		ΔE [eV]	$f(r)$	ΔE [eV]	λ_{\max}^a	$f(r)$
$1^1A'$	ground state	0.00		0.00		
$1^1A''$	$n_S \rightarrow \pi_L^*$	1.80	0.0000	2.55		0.0018
$2^1A'$	$\pi_H \rightarrow \pi_L^*$	2.35	0.5056	2.50	2.52 eV (492 nm)	0.5265
$2^1A''$	$n_N \rightarrow \pi_L^*$	3.22	0.0017	3.49		0.0093
$3^1A'$	$\pi_{H-2} \rightarrow \pi_L^*$	3.26	0.0890	3.23	3.18 eV (390 nm)	0.1724
$1^3A'$	$\pi_H \rightarrow \pi_L^*$	1.68		1.91		
$1^3A''$	$n_S \rightarrow \pi_L^*$	1.74		2.49		
$2^3A'$	$\pi_{H-2} \rightarrow \pi_L^*$	2.71		2.64		
$3^3A'$	$\pi_{H-3} \rightarrow \pi_L^*$	2.92		2.95		

^aAbsorption maxima in 0.1 N phosphate buffer (pH 7), ref 17.

states are smaller than that of the ground state (see Table S4 of the SI for details), with consequences for the differential stabilization by polar solvents (see below). Excitations from the n_N MO are located in a similar energy region as in LF. A medium strong $^1(\pi_{H-2} \rightarrow \pi_L^*)$ transition and a strong transition of mixed $^1(\pi \rightarrow \pi^*)$ origin are found in the UVA region of the absorption spectrum. In the triplet manifold the order of states is reversed with respect to the singlets. Because of the larger exchange interaction between π and π^* MOs as compared to $n\pi^*$ exchange interactions, the $^3(\pi_H \rightarrow \pi_L^*)$ state constitutes the T_1 ($1^3A'$) state but its energy separation to the $^3(n_S \rightarrow \pi_L^*)$ is small. Both triplet states are located energetically below the S_1 ($1^1A''$) state in the vertical excitation spectrum and are thus expected to play an important role in its decay dynamics.

Upon geometry relaxation, the S_1 , S_2 ($2^1A'$), T_1 and T_2 ($1^3A''$) states are stabilized by about 0.3–0.4 eV while the order of states is preserved (Table 2). Their PEHs have true minima at C_s symmetric structures and their geometry parameters are found to be very similar (Table S3 of the SI). This is a consequence of the fact that both the n_S and π_H orbitals from which the excitations originate are dominated by nonbonding

Table 2. Adiabatic DFT/MRCI Excitation Energies [eV] of 2T-LF in the Gas Phase and in Water Solution

state	electronic structure	gas phase	water solution ^a
¹ A''	$n_S \rightarrow \pi_L^*$	1.44	2.19
² A'	$\pi_H \rightarrow \pi_L^*$	1.95	2.10
¹ A'	$\pi_H \rightarrow \pi_L^*$	1.39	1.62
¹ A''	$n_S \rightarrow \pi_L^*$	1.40	2.15

^aValues were obtained by adding the solvent shift at the S_0 geometry to the adiabatic excitation energy of the isolated molecule.

sulfur in-plane and out-of-plane 3p orbitals, respectively. The only substantial differences between both minimum nuclear arrangements are found for the N_5-C_{5a} , $C_{5a}-C_{9a}$ and C_7-C_8 bonds where the π_H MO exhibits some electron density whereas the n_S orbital does not. Adiabatic excitation energies are presented in Table 2, information on the energies of further states at the excited-state minima can be found in Table S4 of the SI. It appears that the geometry optimization at the TDDFT level employing the B3-LYP functional slightly overshoots for the singlet excited states since the lowest DFT/MRCI energy of the S_2 state is found at the TDDFT-optimized S_1 minimum and not at the S_2 minimum. In the corresponding triplet states, T_1 and T_2 , the differences of the geometry parameters are less pronounced. Major changes with respect to the ground-state minimum geometry involve the C_2-S bond which is elongated by about 8 pm and the neighboring C_2-N_1 and C_2-N_3 bonds which are shortened by 3–5 pm. As may be expected from the bonding and antibonding characteristics of the π_L^* MO, the C_4-C_{4a} and $C_{4a}-C_{10a}$ bonds contract in the excited states whereas the neighboring $C_{4a}-N_5$ bond is elongated.

To summarize, in contrast to LF, the $^1(\pi_H \rightarrow \pi_L^*)$ state is not the lowest-lying excited singlet state of 2T-LF in the gas phase. We find the dark $^1(n_S \rightarrow \pi_L^*)$ state approximately 0.5 eV below. Fluorescence will thus be very weak or absent in this compound in the gas phase or apolar solvents. Due to the larger exchange splitting in $\pi\pi^*$ states as compared to $n\pi^*$ states, the $^3(\pi_H \rightarrow \pi_L^*)$ and $^3(n_S \rightarrow \pi_L^*)$ minima are nearly degenerate.

Solvent Effects. The influence of the solvent on the minimum geometries is found to be rather small. As may be seen from Table S3 of the SI most of the bond lengths experience changes below 1 pm when the states are reoptimized for a cluster containing four explicit water molecules. Due to hydrogen bond formation, the $C_4=O$ bond is elongated by 1.6 pm in the singlet states and by 1.8 pm in the T_1 state. The minimum of the T_2 state of the water cluster could not be optimized at the TDDFT/B3-LYP level. The increase of the $C_4=O$ bond lengths goes along with a shortening of the neighboring N_3-C_4 and C_4-C_{4a} bonds.

The lowest-lying absorption band of natural flavins is known to be nearly unaffected by the polarity or the proticity of the solvent.⁴⁶ In contrast, the corresponding band of 2T-LF exhibits negative solvatochromism. The reason for the different solvatochromism of the lowest $^1(\pi \rightarrow \pi^*)$ excitation in 2T-LF and LF is the partial charge transfer from $3p_\pi$ at the sulfur center to the ring system in 2T-LF which is missing in the corresponding natural flavin. For example, the absorption maximum of 2-thio-tetra-O-acetylriboflavin shifts from 510 nm in $CHCl_3$ to 496 nm in aqueous solution at pH 7.¹⁷ This trend is corroborated by the results of our calculations. In the microsolvated cluster, the first bright $^1(\pi_H \rightarrow \pi_L^*)$ transition experiences a slight bathochromic shift (see Table S5 of the SI

for details). However, as soon as the electrostatic interaction with the polarizable continuum is switched on, a hypsochromic shift sets in. In our best water model with four explicit water molecules surrounded by a polarizable continuum of relative permittivity $\epsilon_r = 78$, the blue shift of the absorption band with respect to the gas phase amounts to about 0.15 eV (Table 1). Despite the negative solvatochromism, the $^1(\pi_H \rightarrow \pi_L^*)$ state is the lowest-lying singlet state in the Franck–Condon (FC) spectrum of 2T-LF in aqueous solution. Its computed vertical excitation energy (2.50 eV, 495 nm) agrees excellently with the maximum of the first absorption band in 0.1 molar phosphate buffer at pH 7 (492 nm).¹⁷

The huge hypsochromic shift of the $^1(n_S \rightarrow \pi_L^*)$ state (ca. 0.75 eV) is caused primarily by the interaction of the highly polarizable sulfur lone pair with the polar surrounding ($\epsilon_r = 78$). The proticity of the solvent and the concomitant stabilization of the n_O orbital due to hydrogen bonding, which was found to be substantial in LF, is less important for the photophysics of 2T-LF. With respect to its electronic structure, the S_1 state of LF has its correspondence in the S_3 state (S_4 in vacuum). Again, we observe excellent agreement of its computed vertical excitation energy (3.23 eV, 383 nm) with the maximum of the second absorption band at 390 nm.¹⁷ This is true even for the strong absorption band with a maximum at 316 nm. According to our calculations, this band originates from the $S_0 \rightarrow S_7$ transition in aqueous solution (3.98 eV, 311 nm) which is dominated by the $^1(\pi_H \rightarrow \pi_{L+1}^*)$ excitation.

The binding pocket of the LOV domain provides a similar hydrogen bonding network as the four water molecules in our model but a significantly less polar environment than bulk water.¹⁹ The 2T-LF-4H₂O cluster surrounded by a polarizable continuum of relative permittivity $\epsilon_r = 4$ may therefore serve as a realistic model for 2T-LF in the LOV domain. In this environment, the lowest excited singlet state of 2T-LF is predicted to originate from the $^1(n_S \rightarrow \pi_L^*)$ excitation (see Table S5 of the SI for details).

Triplet Formation. Inspection of Table 2 shows that, from an energetic point of view, the T_1 and T_2 states are possible candidates for efficient ISC from S_1 in the gas phase and in solution. Since the S_1 state is of $^1(n_S \rightarrow \pi_L^*)$ type in the gas phase and of $^1(\pi_H \rightarrow \pi_L^*)$ type in solution, SOMEs are given for all relevant ISC combinations in Table 3. From the qualitative El-Sayed rules,⁴⁷ electronic spin–orbit coupling is expected to be strong only when a change of orbital angular momentum

Table 3. 2T-LF: Calculated Spin–Orbit Matrix Elements $|\langle i|\hat{H}_{SO}|f\rangle|$ [cm^{−1}] Evaluated at the Minimum of the Initial Singlet State, Adiabatic Electronic Energy Differences ΔE^{ad} [cm^{−1}], and ISC Rate Constants k_{ISC} [s^{−1}] in the Gas Phase and Water Solution (See Text)

channel		SOME	rate
$i \rightsquigarrow f$	ΔE^{ad}	$ \langle i \hat{H}_{\text{SO}} f\rangle $	k_{ISC}
$1(n_{\text{S}} \rightarrow \pi_{\text{L}}^*) \rightsquigarrow {}^3(\pi_{\text{H}} \rightarrow \pi_{\text{L}}^*)_{\text{x}}$		160.5	
$1(n_{\text{S}} \rightarrow \pi_{\text{L}}^*) \rightsquigarrow {}^3(\pi_{\text{H}} \rightarrow \pi_{\text{L}}^*)_{\text{y}}$		4.4	
$1(n_{\text{S}} \rightarrow \pi_{\text{L}}^*) \rightsquigarrow {}^3(\pi_{\text{H}} \rightarrow \pi_{\text{L}}^*)_{\text{z}}$		0.0	
$1(\pi_{\text{H}} \rightarrow \pi_{\text{L}}^*) \rightsquigarrow {}^3(n_{\text{S}} \rightarrow \pi_{\text{L}}^*)_{\text{x}}$		135.8	
$1(\pi_{\text{H}} \rightarrow \pi_{\text{L}}^*) \rightsquigarrow {}^3(n_{\text{S}} \rightarrow \pi_{\text{L}}^*)_{\text{y}}$		2.3	
$1(\pi_{\text{H}} \rightarrow \pi_{\text{L}}^*) \rightsquigarrow {}^3(n_{\text{S}} \rightarrow \pi_{\text{L}}^*)_{\text{z}}$		0.0	
$\{\text{S}_1 \rightsquigarrow \text{T}_1\}_{\text{vac}}$	409		$\sim 5 \times 10^{12}$
$\{\text{S}_1 \rightsquigarrow \text{T}_2\}_{\text{wat}}$	−433		$\sim 7 \times 10^{11a}$

^aAt 298 K.

takes place. For this reason, direct ISC is expected to be fast for $^1(n_S \rightarrow \pi_L^*) \leftrightarrow ^3(\pi_H \rightarrow \pi_L^*)$ and for $^1(\pi_H \rightarrow \pi_L^*) \leftrightarrow ^3(n_S \rightarrow \pi_L^*)$. In these states, a substantial part of the unpaired spin-density is located at the sulfur center. Hence, SOMEs are considerably larger than for the parent compound where the spin density in the S_1 $^1(\pi_H \rightarrow \pi_L^*)$ state is delocalized.

As noted above, the geometry parameters of the low-lying excited-state minima are quite similar. This means that we expect the rate constant to obey the energy gap law for the weak coupling case,⁴⁸ i.e., to decrease exponentially with increasing energy separation. When computing these rates, we have assumed that the electronic SOMEs and the shapes of the PEHs do not change substantially by solvent effects. The energy gap between the S_1 and T_1 minima is small in the vacuum (below 500 cm^{-1}) and increases from $\sim 3500 \text{ cm}^{-1}$ in a protic, but only slightly polar medium to $\sim 4600 \text{ cm}^{-1}$ in water. Accordingly, the fast $^1(n_S \rightarrow \pi_L^*) \leftrightarrow ^3(\pi_H \rightarrow \pi_L^*)$ ISC in vacuum proceeding at about $5 \times 10^{12} \text{ s}^{-1}$ slows down by more than 2 orders of magnitude to about $1 \times 10^{10} \text{ s}^{-1}$. In aqueous solution, this process will presumably play a minor role because the $^1(n_S \rightarrow \pi_L^*)$ is only the second excited singlet in that medium.

In contrast, the energy gap between the S_2 and T_2 states shrinks in polar solvents. We obtain a rate constant of $5 \times 10^{11} \text{ s}^{-1}$ for the $^1(\pi_H \rightarrow \pi_L^*) \leftrightarrow ^3(n_S \rightarrow \pi_L^*)$ ISC in vacuum, but internal conversion (IC) to the $^1(n_S \rightarrow \pi_L^*)$ state followed by ISC to the $^3(\pi_H \rightarrow \pi_L^*)$ will be the prevailing decay channel after photoexcitation in the gas phase. In water solution, we obtain a small negative ($\sim -400 \text{ cm}^{-1}$) energy gap for minima of the $^1(\pi_H \rightarrow \pi_L^*)$ and $^3(n_S \rightarrow \pi_L^*)$ pair of states in water. Since the zero-point vibrational energies are similar in both potential wells, the ISC would thus be forbidden at 0 K. At room temperature and assuming a Boltzmann population of the vibrational levels in the initial electronic state, an ISC rate of $\sim 7 \times 10^{11} \text{ s}^{-1}$ is obtained for $^1(\pi_H \rightarrow \pi_L^*) \leftrightarrow ^3(n_S \rightarrow \pi_L^*)$. The radiationless decay to the triplet manifold is much faster than a radiative transition back to the ground state which occurs at rate of $\sim 6 \times 10^7 \text{ s}^{-1}$. Moreover, since conical intersections with the ground state potential energy surface have not been found in the vicinity of the S_1 minimum, we may suppose that internal conversion to the electronic ground state cannot compete either with fast intersystem crossing. Hence, we expect a triplet quantum yield close to unity in 2T-LF and fluorescence to be quenched, both in vacuum and solution.

Triplet Lifetime. Due to the heavy atom effect, thiocarbonyl compounds are expected to exhibit more pronounced phosphorescence and thus an intrinsically shorter triplet lifetime than their carbonyl counterparts. This has indeed been observed in many cases.⁴⁹ In the present context, the question arises whether the T_1 state of 2T-LF is sufficiently long-lived to undergo bimolecular photochemical reactions, in particular the bond formation with the neighboring cysteine residue in the LOV domain.

In the gas phase, the T_1 $^3(\pi_H \rightarrow \pi_L^*)$ state splits into two lower-lying near degenerate sublevels under the influence of spin-orbit coupling and a third sublevel approximately 11 cm^{-1} above. The two lower fine-structure substates exhibit substantial contributions from the T_2 $^3(n_S \rightarrow \pi_L^*)$ state owing to the large SOME and the small energy separation between these states. In contrast, the coefficients of singlet configuration state functions in the spin-orbit mixed wave functions of these substates are tiny. Likewise, the triplet admixture to the electronic ground state wave function is marginal. Our calculations predict the phosphorescence lifetime of these sublevels at cryogenic

temperatures to be approximately 20 s. The higher-lying T_1 fine-structure component mixes strongly with the S_1 $^1(n_S \rightarrow \pi_L^*)$ state. Intensity borrowing from the (relatively weak) $S_1 \rightarrow S_0$ emission yields a phosphorescence rate constant of about 10 s^{-1} for this level, corresponding to a lifetime of 100 ms. Assuming equal populations of the three sublevels yields a high-temperature limit of 3.6 s^{-1} for the radiative decay rate, corresponding to an average T_1 phosphorescence lifetime of 280 ms.

In aqueous solution, the probability for a phosphorescence decay of the T_1 state is expected to be even smaller than in the gas phase because of the hypsochromic shifts of the perturbing ($n_S \rightarrow \pi_L^*$) states. We therefore conclude that the T_1 state of 2T-LF is sufficiently long-lived to undergo photochemical reactions.

4-Thio-lumiflavin. Vacuum. Also the 4T-LF isomer exhibits a planar nuclear arrangement of the ring system in the electronic ground state. Selected bond lengths are displayed in Table S6 of the SI. Again, only slight changes of the geometry parameters are observed when comparing 4T-LF with LF. In the neighborhood of $C_4=S$ bond, the N_3-C_4 and C_4-C_{4a} bonds slightly contract with respect to LF. All other geometry parameters are nearly unchanged.

The frontier MOs of 4T-LF resemble those of 2T-LF both with respect to energetic order and shape when the oxygen and sulfur centers are interchanged (Figure 4). The π_H and π_{L+2}^* MOs in 4T-LF just appear somewhat more delocalized. In the singlet manifold, the lowest excited state corresponds to a $^1(n_S \rightarrow \pi_L^*)$ excitation with negligible oscillator strength (Table 4).

Table 4. Vertical Excitation Spectra of 4T-LF in the Gas Phase and in Water Solution

state	electronic structure	gas phase		water solution		
		ΔE [eV]	$f(r)$	ΔE [eV]	λ_{max}^a	$f(r)$
$1^1A'$	ground state	0.00		0.00		
$1^1A''$	$n_S \rightarrow \pi_L^*$	1.72	0.0000	2.40	2.34 (530 nm) ^b	0.0000
$2^1A'$	$\pi_H \rightarrow \pi_L^*$	2.62	0.3767	2.57	2.51 (494 nm)	0.3952
$3^1A'$	$\pi_{H-2} \rightarrow \pi_L^*$	3.07	0.0610	3.11	3.14 (368 nm)	0.0528
$2^1A''$	$n_N \rightarrow \pi_L^*$	3.16	0.0019	3.40		0.0016
$1^3A''$	$n_S \rightarrow \pi_L^*$	1.61		2.29		
$1^3A'$	$\pi_H \rightarrow \pi_L^*$	1.84		1.99		
$2^3A'$	$\pi_{H-2} \rightarrow \pi_L^*$	2.44		2.49		
$2^3A''$	$n_N \rightarrow \pi_L^*$	2.83		3.07		

^aAbsorption maxima in 0.1 N phosphate buffer (pH 7), ref 17.

^bShoulder in absorption spectrum in 0.1 N phosphate buffer (pH 7), ref 17.

Its excitation energy is comparable to the corresponding state in 2T-LF while its dipole moment is even more reduced with respect to the electronic ground state (see Table S7 of the SI). Like in 2T-LF, the optically bright $^1(\pi_H \rightarrow \pi_L^*)$ excitation is associated with the $S_2 \rightarrow S_0$ transition. However, despite its higher excitation energy, its oscillator strength ($f(r) \approx 0.38$) is smaller than the corresponding transition in 2T-LF. We find the electric dipole moment of S_2 to be nearly unchanged with respect to the electronic ground state. Hence, we expect no or small solvatochromism of this band in polar solvents (see Section). The S_3 and S_4 states have reversed order in the FC spectrum of both isomers. While the $^1(n_N \rightarrow \pi_L^*)$ excitation is

located in a similar energy range as in 2T-LF and LF, the medium strong $^1(\pi_{\text{H}-2} \rightarrow \pi_{\text{L}}^*)$ transition is found at substantially lower excitation energies (3.07 eV) in 4T-LF than in 2T-LF (3.26 eV) and in LF (3.84 eV).¹⁸

The order of states in the triplet manifold is the same as in the singlet manifold but the energy gap between the $^3(n_{\text{S}} \rightarrow \pi_{\text{L}}^*)$ and $^3(\pi_{\text{H}} \rightarrow \pi_{\text{L}}^*)$ is considerably smaller than between the corresponding singlet states. In contrast to 2T-LF, the $^3(\pi_{\text{S}} \rightarrow \pi_{\text{L}}^*)$ excitation yields the lowest triplet state in 4T-LF in the gas phase. In the FC region, even a third triplet state, $^3(\pi_{\text{H}-2} \rightarrow \pi_{\text{L}}^*)$, is located energetically below the bright S_2 state and might thus be important for the photophysics of 4T-LF.

The largest geometrical changes between the ground- and excited-state geometries (Table S6 of the SI) are observed in the pteridine-ring. The similarities between the excited-state geometries are much less pronounced than in the 2T-LF isomer. This may be a consequence of the fact that the π_{H} MO is not so strongly localized at the sulfur center in 4T-LF as the n_{S} orbital. The $\text{N}_1\text{--C}_2$ bond, for instance, is shortened in the S_1 state with regard to the electronic ground state whereas it is elongated in the T_2 state. Particularly the extremely large change of the $\text{C}_2\text{--N}_3$ bond length in the S_2 state by almost 15 pm catches the eye. Again, it appears that the geometry distortions in the S_2 state are too pronounced at the TDDFT(B3-LYP) level, since the DFT/MRCI energy at the S_2 geometry (2.44 eV) is higher by 0.11 eV than at the S_1 and T_1 minimum nuclear arrangements (Table S7 of the SI). TDDFT(B3-LYP) yields a slightly out-of-plane distorted minimum nuclear arrangement in the latter T_1 state, the deviations of dihedral angles from planarity being below 1° . It turns out, however, that the DFT/MRCI method favors the planar structure by 38 cm^{-1} . The geometry parameters of the T_3 minimum are characterized by a simultaneous elongation of the $\text{C}_2\text{=O}$ and $\text{C}_4\text{=S}$ as may be expected from the density distribution in the $\pi_{\text{H}-2}$ MO. In addition, the $\text{C}_{4a}\text{--N}_5$ is stretched by about 4 pm, characteristic of the occupation of the π_{L}^* MO.

The adiabatic energy difference between the S_1 and S_2 states of 4T-LF amounts to nearly 1 eV (Table 5) and is thus

Table 5. Adiabatic DFT/MRCI Excitation Energies [eV] of 4T-LF in the Gas Phase and in Water Solution

state	electronic structure	gas phase	water solution ^a
$1^1\text{A}''$	$n_{\text{S}} \rightarrow \pi_{\text{L}}^*$	1.47	2.13
$2^1\text{A}'$	$\pi_{\text{H}} \rightarrow \pi_{\text{L}}^*$	2.44	2.39
$1^3\text{A}''$	$n_{\text{S}} \rightarrow \pi_{\text{L}}^*$	1.35	2.03
$1^3\text{A}'$	$\pi_{\text{H}} \rightarrow \pi_{\text{L}}^*$	1.55	1.70
$2^3\text{A}'$	$\pi_{\text{H}-2} \rightarrow \pi_{\text{L}}^*$	2.33	2.38

^aValues were obtained by adding the solvent shift at the S_0 geometry to the adiabatic excitation energy of the isolated molecule.

substantially larger than in the 2T-LF isomer. The T_1 and T_2 states are stabilized by about 0.3 eV upon geometry relaxation. Both are located energetically below the S_1 and S_2 states in the gas phase. The S_2 and T_3 minima are found to be near degenerate. This fact may gain importance in polar solvents where the $^1,^3(n_{\text{S}} \rightarrow \pi_{\text{L}}^*)$ states are expected to experience strong blue shifts.

Solvent Effects. It might be expected that the largest change of the geometry parameters with respect to the vacuum structure would occur for the $\text{C}_2\text{=O}$ bond due to the formation of strong hydrogen bonds. This is not what is

observed, however, in the electronic ground state of the 4T-LF·4H₂O cluster. Interestingly, the $\text{C}_4\text{=S}$ bond is elongated by 2 pm while the neighboring $\text{N}_3\text{--C}_4$ bond shrinks by 1.6 pm. All other bond length changes due to water solvation are below 1 pm. On the basis of our results for 2T-LF·4H₂O (see above) we have refrained from optimizing the excited state structures of 4T-LF·4H₂O. Instead, adiabatic energies obtained in vacuum will be combined with solvent shifts computed at the ground state geometry to estimate adiabatic energies in solution.

The solvent effects on the vertical excitation spectrum of 4T-LF (Table S8 of the SI) are less pronounced than those of the 2T-LF isomer. From the analysis of the electric dipole moments this was to be expected for the $\pi_{\text{H}} \rightarrow \pi_{\text{L}}^*$ excitations, but the smaller blue shift of the $n_{\text{S}} \rightarrow \pi_{\text{L}}^*$ excited states of 4T-LF came as a surprise. The $^1,^3(n_{\text{S}} \rightarrow \pi_{\text{L}}^*)$ states experience hypsochromic shifts of ~ 0.4 eV in aqueous solution. The differential solvent effects are thus not sufficient to push the $^1(\pi_{\text{S}} \rightarrow \pi_{\text{L}}^*)$ minimum energetically above the $^1(\pi_{\text{H}} \rightarrow \pi_{\text{L}}^*)$ minimum. The $^1(n_{\text{S}} \rightarrow \pi_{\text{L}}^*)$ state therefore remains to be the first excited singlet state even in aqueous solution (Table 4). Tentatively, we attribute the shoulder at 530 nm (2.34 eV) observed in the experimental absorption spectrum¹⁷ to the $\text{S}_1 \rightarrow \text{S}_0$ electronic transition for which we obtain a value of 2.40 eV in aqueous solution. The maximum of this absorption band at 494 nm (2.51 eV)¹⁷ fits well to the computed vertical excitation energy of the $\text{S}_2 \rightarrow \text{S}_0$ transition (2.57 eV). Likewise, we assign the second absorption band with maximum at 368 nm (3.14 eV)¹⁷ to the $\text{S}_3 \rightarrow \text{S}_0$ transition (theoretical value 3.11 eV) which is dominated by the $^1(\pi_{\text{H}-2} \rightarrow \pi_{\text{L}}^*)$ excitation.

In the triplet manifold, the energy gap between the corresponding $^3(n_{\text{S}} \rightarrow \pi_{\text{L}}^*)$ and $^3(\pi_{\text{H}} \rightarrow \pi_{\text{L}}^*)$ minima in vacuum is much smaller than between the corresponding singlet states. In this case, the interaction with the polar environment is sufficient to reverse the energetic order of the triplet states. Thus, in water the T_1 state is characterized by a $^3(\pi_{\text{H}} \rightarrow \pi_{\text{L}}^*)$ electronic structure with the T_2 $^3(n_{\text{S}} \rightarrow \pi_{\text{L}}^*)$ state close by. The T_3 state experiences a small blue shift with respect to vacuum, but remains in the same energy range as the S_2 state.

Intersystem Crossing. Since the S_1 state of 4T-LF clearly exhibits $^1(n_{\text{S}} \rightarrow \pi_{\text{L}}^*)$ character in vacuum and polar protic environments (Table 5), we have refrained from computing rates for the $^1(\pi_{\text{H}} \rightarrow \pi_{\text{L}}^*)$ decay via ISC. Instead, it is assumed that a fast internal conversion to the S_1 state takes place. In vacuum and at low temperatures, the $^1(n_{\text{S}} \rightarrow \pi_{\text{L}}^*) \rightsquigarrow ^3(\pi_{\text{H}} \rightarrow \pi_{\text{L}}^*)$ channel is energetically not available (Table 6). Our calculations place the $^3(\pi_{\text{H}} \rightarrow \pi_{\text{L}}^*)$ state adiabatically 615 cm^{-1} above the minimum of the S_1 state. In principle, the $^1(n_{\text{S}} \rightarrow \pi_{\text{L}}^*)$

Table 6. 4T-LF: Calculated Spin–Orbit Matrix Elements $|\langle i|\hat{H}_{\text{SO}}|f\rangle|$ [cm^{−1}] Evaluated at the Minimum of the Initial Singlet State, Adiabatic Electronic Energy Differences ΔE^{ad} [cm^{−1}], and ISC Rate Constants k_{ISC} [s^{−1}] in the Gas Phase and Water Solution (See Text)

channel	ΔE^{ad}	SOME $ \langle i \hat{H}_{\text{SO}} f\rangle $	rate k_{ISC}
$i \rightsquigarrow f$			
$^1(n_{\text{S}} \rightarrow \pi_{\text{L}}^*) \rightsquigarrow ^3(\pi_{\text{H}} \rightarrow \pi_{\text{L}}^*)_{\text{x}}$		−73.1	
$^1(n_{\text{S}} \rightarrow \pi_{\text{L}}^*) \rightsquigarrow ^3(\pi_{\text{H}} \rightarrow \pi_{\text{L}}^*)_{\text{y}}$		−141.7	
$^1(n_{\text{S}} \rightarrow \pi_{\text{L}}^*) \rightsquigarrow ^3(\pi_{\text{H}} \rightarrow \pi_{\text{L}}^*)_{\text{z}}$		0.0	
$\{\text{S}_1 \rightsquigarrow \text{T}_2\}_{\text{vac}}$	−615		$\sim 1.5 \times 10^{12\text{at}}$
$\{\text{S}_1 \rightsquigarrow \text{T}_1\}_{\text{wat}}$	3663		$\sim 1.3 \times 10^{12}$

^aAt 298 K.

state of 4T-LF could decay radiationlessly to the $^3(n_S \rightarrow \pi_L^*)$ state via ISC. According to the El-Sayed rules, this transition is forbidden because it is not accompanied by a change of orbital angular momentum, but it could borrow intensity by vibronic coupling with the nearby $(\pi_H \rightarrow \pi_L^*)$ states. Vibronic spin-orbit coupling has not been taken into account in this work. Once the much faster El-Sayed allowed ISC is energetically available, vibronic spin-orbit coupling is assumed to play a minor part. Population of higher vibrational levels in the S_1 potential well at room temperature leads to very fast $^1(n_S \rightarrow \pi_L^*) \rightsquigarrow ^3(\pi_H \rightarrow \pi_L^*)$ decay at the picosecond time scale. In aqueous solution, where the energy separation between these states is larger, the $^1(n_S \rightarrow \pi_L^*) \rightsquigarrow ^3(\pi_H \rightarrow \pi_L^*)$ ISC proceeds at about $1.3 \times 10^{12} \text{ s}^{-1}$. Hence, we expect a triplet quantum yield close to unity in 4T-LF and fluorescence to be quenched in solution. In the gas phase, ISC from the lowest singlet state is predicted to be an activated process.

We have refrained from computing phosphorescence lifetimes because similar orders of magnitude are expected as for 2T-LF.

2,4-Dithio-lumiflavin. Vacuum. Also the 2,4DT-LF molecule exhibits a planar nuclear arrangement of the ring system in the electronic ground state. (For geometry parameters see Table S9 of the SI.) Similar trends as in the monothiosubstituted compounds are observed: Introduction of the C=S groups is accompanied by a slight contraction of the neighboring C–N and/or C–C bonds while all other geometry parameters are nearly unchanged with respect to the parent compound.

The HOMO and HOMO-1 of 2,4DT-LF (Figure 5) are very similar to those of 2T-LF while HOMO-2 and HOMO-3

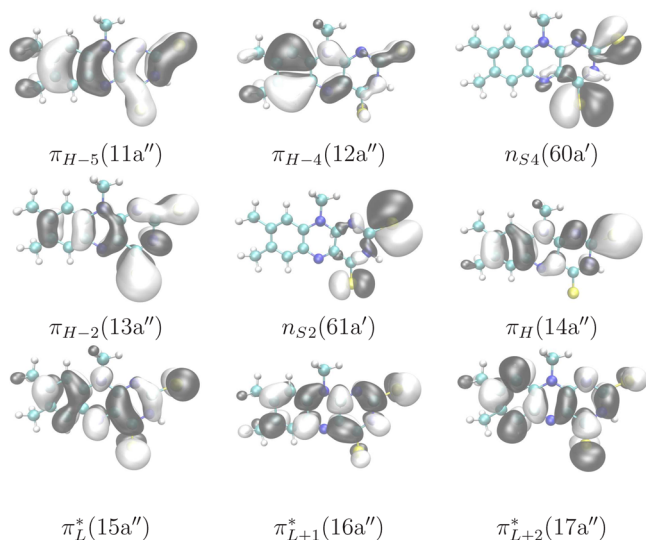


Figure 5. Frontier orbitals of 2,4DT-LF at the optimized ground-state geometry. (Isovalue = 0.02.)

resemble the HOMO and HOMO-1 of 4T-LF. Occupation of the $3p_\pi$ and n orbitals at the S_4 center is thus energetically preferred over the corresponding orbitals at the S_2 center. The π_{H-4} MO with high electron density in the benzene ring plays only a minor role for the lowest-lying electronic states of 2,4DT-LF. Interestingly, σ -type orbitals with lone-pair character at the nitrogen atoms are not among the six highest occupied MOs of 2,4DT-LF. The LUMO, LUMO+1, and LUMO+2

exhibit qualitatively the same shape as in all lumiflavin derivatives investigated in this work.

In accord with the energetic order of the MOs, $(n_N \rightarrow \pi_L^*)$ states are not among the low-lying excited states of 2,4DT-LF (Table 7). In vacuum, the first two excited singlet states are

Table 7. Vertical Excitation Spectra of 2,4DT-LF in the Gas Phase and in Water Solution

state	electronic structure	gas phase		water solution	
		ΔE [eV]	$f(r)$	ΔE [eV]	$f(r)$
$1^1A'$	ground state	0.00		0.00	
$1^1A''$	$n_{S2} \rightarrow \pi_L^*$	1.57	0.0000	2.22	0.0001
$2^1A''$	$n_{S4} \rightarrow \pi_L^*$	1.83	0.0000	2.45	0.0045
$2^1A'$	$\pi_H \rightarrow \pi_L^*$	2.20	0.3839	2.32	0.3952
$3^1A'$	$\pi_{H-2} \rightarrow \pi_L^*$	2.52	0.2519	2.73	0.1742
$1^3A''$	$n_{S2} \rightarrow \pi_L^*$	1.49		2.13	
$1^3A'$	$\pi_H \rightarrow \pi_L^*$	1.62		1.77	
$2^3A''$	$n_{S4} \rightarrow \pi_L^*$	1.77		2.40	
$2^3A'$	$\pi_{H-2} \rightarrow \pi_L^*$	1.81		2.20	

linear combinations of $(n_{S2} \rightarrow \pi_L^*)$ and $(n_{S4} \rightarrow \pi_L^*)$ excitations. The transitions carry only tiny electric dipole oscillator strengths and hence are expected to be dark. In contrast, strong absorption is predicted for the $S_3 \leftarrow S_0$ and $S_4 \leftarrow S_0$ transitions dominated by the $^1(\pi_H \rightarrow \pi_L^*)$ and $^1(\pi_{H-2} \rightarrow \pi_L^*)$ excitations, respectively. We found a nonplanar minimum structure in the T_1 $^3(n_S \rightarrow \pi_L^*)$ state of 2,4DT-LF. The deviations from planarity are minimal (i.e., $< 1^\circ$), however. The $^3(\pi_H \rightarrow \pi_L^*)$ configuration dominates the T_2 state in vacuum, while the second $^3(n_S \rightarrow \pi_L^*)$ state has moved to the T_3 PEH. Otherwise, the electronic structures of the low-lying singlet and triplet states resemble each other closely (Table 7 and Table S10 of the SI).

Solvent Effects. Vertical excitation energies for various solvent environments are displayed in Table S11 of the SI. To our knowledge, experimental absorption spectra are not available for this compound or related ones. In aqueous solution of 2,4DT-LF (Table 7), the first intense absorption maximum is predicted to occur at 2.32 eV (534 nm). It originates from the $^1(\pi_H \rightarrow \pi_L^*)$ excitation. In the vertical spectrum, the lowest singlet excited state is still due to the $^1(n_S \rightarrow \pi_L^*)$ transition, despite a huge blue shift of the transition wavelength with respect to the gas-phase value. Adiabatically, the order of states appears to be reversed because the relaxation is found to be larger in the $^1(\pi_H \rightarrow \pi_L^*)$ state. Assuming relaxation and solvent effects to be additive, an estimated value of 1.95 eV is obtained for the adiabatic $^1(\pi_H \rightarrow \pi_L^*)$ excitation energy (Table 8). The minimum of the $^1(n_S \rightarrow \pi_L^*)$ PEH is estimated to lie approximately 0.08 eV higher at about 2.03 eV.

Table 8. Adiabatic DFT/MRCI Excitation Energies [eV] of 2,4DT-LF in the Gas Phase and in Water Solution

state	electronic structure	gas phase	water solution ^a
$1^1A''$	$n_{S2} \rightarrow \pi_L^*$	1.38	2.03
$2^1A''$	$n_{S4} \rightarrow \pi_L^*$	1.63	2.25
$2^1A'$	$\pi_H \rightarrow \pi_L^*$	1.83	1.95
$1^3A''$	$n_{S2} \rightarrow \pi_L^*$	1.33	1.97
$1^3A'$	$\pi_H \rightarrow \pi_L^*$	1.38	1.53

^aValues were obtained by adding the solvent shift at the S_0 geometry to the adiabatic excitation energy of the isolated molecule.

Due to the close proximity of these two singlet states, their vibronic interaction is supposed to be substantial. For the second $^1(n_S \rightarrow \pi_L^*)$ state, an adiabatic excitation energy of 2.25 eV is predicted.

A polar protic environment changes the order of triplet states with respect to the gas phase. The lowest triplet state clearly arises from the $^3(\pi_H \rightarrow \pi_L^*)$ in water solution. The lower of the two $^3(n_S \rightarrow \pi_L^*)$ states is found to be almost degenerate with the $^1(\pi_H \rightarrow \pi_L^*)$ state under these conditions (Table 8).

Intersystem Crossing. An overview over the calculated ISC rates of photoexcited 2,4DT-LF can be obtained from Table 9.

Table 9. 2,4DT-LF: Calculated Spin–Orbit Matrix Elements $|\langle i|\hat{H}_{SO}|f\rangle|$ [cm^{-1}] Evaluated at the Minimum of the Initial Singlet State, Adiabatic Electronic Energy Differences ΔE^{ad} [cm^{-1}], and ISC Rate Constants k_{ISC} [s^{-1}] in the Gas Phase and Water Solution (See Text)

channel		SOME	rate
$i \rightsquigarrow f$	ΔE^{ad}	$ \langle i \hat{H}_{SO} f\rangle $	k_{ISC}
$^1(n_S \rightarrow \pi_L^*) \rightsquigarrow ^3(\pi_H \rightarrow \pi_L^*)_x$		−156.2	
$^1(n_S \rightarrow \pi_L^*) \rightsquigarrow ^3(\pi_H \rightarrow \pi_L^*)_y$		−1.4	
$^1(n_S \rightarrow \pi_L^*) \rightsquigarrow ^3(\pi_H \rightarrow \pi_L^*)_z$		0.0	
$^1(\pi_H \rightarrow \pi_L^*) \rightsquigarrow ^3(n_S \rightarrow \pi_L^*)_x$		−126.1	
$^1(\pi_H \rightarrow \pi_L^*) \rightsquigarrow ^3(n_S \rightarrow \pi_L^*)_y$		12.2	
$^1(\pi_H \rightarrow \pi_L^*) \rightsquigarrow ^3(n_S \rightarrow \pi_L^*)_z$		0.0	
$\{S_1 \rightsquigarrow T_2\}_{\text{vac}}$	−35		$\sim 8.1 \times 10^{12\text{a}}$
$\{S_1 \rightsquigarrow T_2\}_{\text{wat}}$	−94		$1 \times 10^{12\text{a}}$

^aAt 298 K.

In the gas phase, $S_1 \rightsquigarrow T_1$ ISC is El-Sayed forbidden. Due to the near-degeneracy of the S_1 and T_2 states, we find the El-Sayed allowed nonradiative decay of the S_1 state to proceed at the subpicosecond time scale from vibrationally excited levels of the initial electronic state. Accordingly, a triplet yield close to 1.0 is expected at room temperature.

In water solution, the situation is reversed. Here, the $^1(\pi_H \rightarrow \pi_L^*)$ excitation constitutes the S_1 state that is nearly degenerate with the $^3(n_S \rightarrow \pi_L^*)$ T_2 state. At room temperature, we obtain a rate constant of $1 \times 10^{12} \text{ s}^{-1}$ for the $S_1 \rightsquigarrow T_1$ ISC. Since the rate for a radiative decay of the S_1 state is more than 3 orders of magnitude smaller than k_{ISC} , fluorescence cannot compete with triplet formation.

SUMMARY AND CONCLUSIONS

In this work, we have investigated the absorption characteristics and excited-state decay mechanisms of various lumiflavin derivatives using advanced quantum chemical methods. We find three thiocarbonyl compounds, the monosubstituted 2T-LF and 4T-LF as well as the disubstituted 2,4DT-LF, to have promising photophysical properties. They absorb in the blue-green wavelength regime around 500 nm, i.e., substantially red-shifted with respect to lumiflavin that is the cofactor of natural blue-light photoreceptors. While in lumiflavin fluorescence and triplet formation compete in polar protic solvents, we expect the triplet quantum yields to be close to unity in the thioflavins. Their first singlet excited state is predicted to decay efficiently via ISC at the picosecond time scale. Their lowest triplet states, on the other hand, are sufficiently long-lived to enable bimolecular photochemical reactions. The combination of these properties makes the thioflavins potentially suitable candidates as cofactors in biomimetic photoswitches.

Figure 6 provides a schematic overview over the primary decay mechanisms following photoexcitation of lumiflavin and

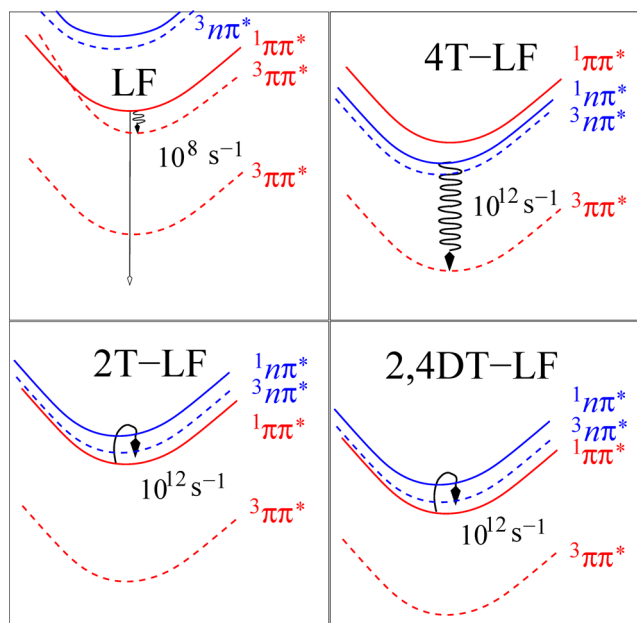


Figure 6. Schematic resume of the triplet formation mechanisms and intersystem crossing rates in water solution in lumiflavin and the thioflavins studied in this work.

the thioflavins in water solution. In previous work on LF¹⁸ it was shown that vibronic spin–orbit coupling has to be invoked to reach the triplet manifold from the initially populated $^1(\pi_H \rightarrow \pi_L^*)$ state. Fluorescence that takes place at a rate of $k_F \approx 5 \times 10^7 \text{ s}^{-1}$ can thus compete with the El-Sayed forbidden ISC proceeding at a rate of $k_{\text{ISC}} \approx 10^8 \text{ s}^{-1}$. We find two major causes that substantially accelerate ISC in thioflavins. The heavy-atom effect increases the size of the spin–orbit matrix elements substantially. At least equally important is the energetic stabilization of the first singlet and triplet $n\pi^*$ states. In 4T-LF, the $^1(n_S \rightarrow \pi_L^*)$ state constitutes the S_1 state even in solution. Photoexcitation to the optically bright S_2 state is followed by fast internal conversion to S_1 and an El-Sayed allowed ISC to the $^3(\pi_H \rightarrow \pi_L^*)$ state at a rate of $k_{\text{ISC}} \approx 10^{12} \text{ s}^{-1}$. In contrast, the optically bright $^1(\pi_H \rightarrow \pi_L^*)$ is the lowest singlet state in aqueous solutions of 2T-LF. Due to the close proximity of the $^3(n_S \rightarrow \pi_L^*)$ state, fluorescence will be efficiently quenched. Our calculations predict the triplet formation to be an activated process proceeding with a rate of $k_{\text{ISC}} \approx 10^{12} \text{ s}^{-1}$ at room temperature. Interestingly, the introduction of a second sulfur atom in the 4-position in 2,4DT-LF lowers the excitation energies of the first and second singlet and triplet states, but it does not alter the decay paths as compared to 2T-LF. Finally, the $^3(\pi_H \rightarrow \pi_L^*)$ character of the T_1 state that is common to all four compounds is responsible for the long triplet lifetime.

The combination of a high triplet quantum yield and a long triplet lifetime is a favorable prerequisite for initiating a photocycle in LOV domains. In contrast to other flavin binding pockets such as BLUF, no aromatic amino acids are found close to the cofactor in LOV domains. Thus, quenching of the excitation by excitation energy or electron transfer is less probable in the latter. Rather, in natural blue-light receptors featuring LOV domains the cofactor is stabilized by a hydrogen-bonding network of the surrounding amino acids. In the course

of the photocycle, the thiol hydrogen of a neighboring cysteine migrates to the N₅ center and a covalent bond is formed between the cysteine sulfur and the carbon atom in C_{4a} position of the isoalloxazine core. As mentioned already in the introduction, LOV domains can be fused to cellular effector proteins to create artificial blue light-sensitive variants enabling photochemical regulation of protein function. For optogenetic control, sensitization by blue light might cause too much harm. Hence, scientists are looking worldwide for triggers that can be stimulated at longer wavelengths. The three thioflavins considered in this work achieve this objective. In addition, the chemical behavior of LF should best be mimicked by 2T-LF since the substitution of a sulfur for a carbonyl oxygen in 2-position of FMN is expected to have only minor influence on the electron density distributions at the rather distant reactive N₅ and C_{4a} centers of the isoalloxazine core. Hence, among the present LF variants, we believe 2T-LF to be the most promising artificial cofactor. Studies investigating the photophysics and photochemistry of thioflavins in the protein environment of LOV domains are currently being undertaken in our laboratories.

■ ASSOCIATED CONTENT

■ Supporting Information

Vertical excitation spectra in vacuum of all compounds at their respective ground-state equilibrium geometries; selected bond lengths of the ground and excited state structures, vertical excitation energies at ground- and excited-state geometries, and environment effects on the excitation energies of all thiolumiflavins. This material is available free of charge via the Internet at <http://pubs.acs.org>.

■ AUTHOR INFORMATION

Corresponding Author

*E-mail: Christel.Marian@uni-duesseldorf.de. Tel.: +49 211 8113210.

Notes

The authors declare no competing financial interest.

■ ACKNOWLEDGMENTS

Financial support by the Deutsche Forschungsgemeinschaft through MA 1051/12-1 is gratefully acknowledged.

■ REFERENCES

- (1) Losi, A. Flavin-Based Blue-Light Photosensors: A Photo-biophysics Update. *Photochem. Photobiol.* **2007**, *83*, 1283–1300.
- (2) Briggs, W. R.; et al. The Phototropin Family of Photoreceptors. *Plant Cell* **2001**, *13*, 993–997.
- (3) Gomelsky, M.; Klug, G. BLUF: A Novel FAD-Binding Domain Involved in Sensory Transduction in Microorganisms. *Trends Biochem. Sci.* **2002**, *10*, 497–500.
- (4) Herrou, J.; Crosson, S. Function, Structure and Mechanism of Bacterial Photosensory LOV Proteins. *Nat. Rev. Microbiol.* **2011**, *9*, 713–723.
- (5) Losi, A.; Gärtner, W. Old Chromophores, New Photoactivation Paradigms, Trendy Applications: Flavins in Blue Light-Sensing Photoreceptors. *Photochem. Photobiol.* **2011**, *87*, 491–510.
- (6) Riggsbee, C. W.; Deiters, A. Recent Advances in Photochemical Control of Protein Function. *Trends Biotechnol.* **2010**, *28*, 468–475.
- (7) Pastrana, E. Optogenetics: Controlling Cell Function with Light. *Nat. Methods* **2011**, *8*, 24–25.
- (8) Drepper, T.; Krauss, U.; zu Berstenhorst, S. M.; Pietruszka, J.; Jaeger, K. E. Lights on and Action! Controlling Microbial Gene Expression by Light. *Appl. Microbiol. Biotechnol.* **2011**, *90*, 23–40.
- (9) Wu, Y. I.; Frey, D.; Lungu, O. I.; Jaehrig, A.; Schlichting, I.; Kuhlman, B.; Hahn, K. M. A Genetically Encoded Photoactivatable Rac Controls the Motility of Living Cells. *Nature* **2009**, *461*, 104–108.
- (10) Kramer, R. H.; Fortin, D. L.; Trauner, D. New Photochemical Tools for Controlling Neuronal Activity. *Curr. Opin. Neurobiol.* **2009**, *19*, 1–9.
- (11) Salzmann, S.; Martinez-Junza, V.; Zorn, B.; Braslavsky, S. E.; Mansurova, M.; Marian, C. M.; Gärtner, W. Photophysical Properties of Structurally and Electronically Modified Flavin Derivatives Determined by Spectroscopy and Theoretical Calculations. *J. Phys. Chem. A* **2009**, *113*, 9365–9375.
- (12) Hecht, S.; Richter, G.; Bacher, A.; Joshi, M.; Römisch, W.; Greiner, G.; Frank, R.; Weber, S.; Eisenreich, W.; Fischer, M. Photocycle of a blue light receptor LOV2 domain reconstituted with 5-deazaFMN. In *Flavins and Flavoproteins 2005; Proceedings of the 15th International Symposium on Flavins and Flavoproteins*; Nishino, T., Miura, R., Tanokura, M., Fukui, K., Eds.; ARchiTect Inc.: Tokyo, 2005; pp 569–574.
- (13) Silva-Junior, M. R. Quantum Mechanical/Molecular Mechanics Study of Electronically Excited States and Assessment of Methods for Calculating Vertical Excitation Energies. Ph.D. Thesis; Heinrich Heine Universität Düsseldorf, 2011.
- (14) Silva-Junior, M. R.; Mansurova, M.; Gärtner, W.; Thiel, W. Photophysics of Structurally Modified Flavin Derivates in the Blue-Light Photoreceptor Ytva: A Combined Experimental and Theoretical Study. *ChemBioChem* **2013**, *14*, 1648–1661.
- (15) Macheroux, P.; Bornemann, S.; Ghisla, S.; Thorneley, R. N. F. Studies with Flavin Analogs Provide Evidence that a Protonated Reduced FMN Is the Substrate-Induced Transient Intermediate in the Reaction of Escherichia Coli Chorismate Synthase. *J. Biol. Chem.* **1996**, *271*, 25850–25858.
- (16) Mansurova, M.; Simon, J.; Salzmann, S.; Marian, C. M.; Gärtner, W. Spectroscopic and Theoretical Study on Electronically Modified Chromophores in LOV Domains: 8-Bromo- and 8-Trifluoromethyl-Substituted Flavins. *ChemBioChem* **2013**, *14*, 645–654.
- (17) Dudley, K. H.; Ehrenberg, A.; Hemmerich, P.; Müller, F. Spektren und Strukturen der am Flavin-Redoxsystem beteiligten Partikeln. Studien in der Flavinreihe IX [1]. *Helv. Chim. Acta* **1964**, *47*, 1354–1382.
- (18) Salzmann, S.; Tatchen, J.; Marian, C. M. The Photophysics of Flavins: What Makes the Difference Between Gas Phase and Aqueous Solution? *J. Photochem. Photobiol. A* **2008**, *198*, 221–231.
- (19) Salzmann, S.; Silva-Junior, M. R.; Thiel, W.; Marian, C. M. Influence of the LOV Domain on Low-Lying Excited States of Flavin: A Combined Quantum-Mechanics/Molecular-Mechanics Investigation. *J. Phys. Chem. B* **2009**, *113*, 15610–15618.
- (20) TURBOMOLE V6.3 2011, a development of University of Karlsruhe and Forschungszentrum Karlsruhe GmbH, 1989–2007, TURBOMOLE GmbH, since 2007; available from <http://www.turbomole.com>.
- (21) Schäfer, A.; Huber, C.; Ahlrichs, R. Fully Optimized Contracted Gaussian Basis Sets of Triple Zeta Valence Quality for Atoms Li to Kr. *J. Chem. Phys.* **1994**, *100*, 5829–5835.
- (22) Becke, A. D. Density-Functional Thermochemistry. 3. The Role of Exact Exchange. *J. Chem. Phys.* **1993**, *98*, 5648–5652.
- (23) Stephens, P. J.; Devlin, F. J.; Chabalowski, C. F.; Frisch, M. J. Ab-Initio Calculation of Vibrational Absorption and Circular-Dichroism Spectra Using Density-Functional Force-Fields. *J. Phys. Chem.* **1994**, *98*, 11623–11627.
- (24) Bauernschmitt, R.; Ahlrichs, R. Treatment of Electronic Excitations within the Adiabatic Approximation of Time-Dependent Density Functional Theory. *Chem. Phys. Lett.* **1996**, *256*, 454–464.
- (25) Furche, F.; Ahlrichs, R. Adiabatic Time-Dependent Density Functional Methods for Excited State Properties. *J. Chem. Phys.* **2002**, *117*, 7433–7447.
- (26) Kind, C.; Reiher, M.; Neugebauer, J. SNF Version 2.2.1: A Program Package for Numerical Frequency Analyses; Universität Erlangen, 1999–2002.

- (27) Grimme, S.; Waletzke, M. A Combination of Kohn-Sham Density Functional Theory and Multi-Reference Configuration Interaction Methods. *J. Chem. Phys.* **1999**, *111*, 5645–5655.
- (28) Becke, A. D. A New Mixing of Hartree-Fock and Local Density Functional Theories. *J. Chem. Phys.* **1993**, *98*, 1372–1377.
- (29) Lee, C.; Yang, W.; Parr, R. G. Development of the Colle-Salvetti Correlation-Energy Formula into a Functional of the Electron Density. *Phys. Rev.* **1988**, *B 37*, 785–789.
- (30) Silva-Junior, M. R.; Schreiber, M.; Sauer, S. P. A.; Thiel, W. Benchmarks for Electronically Excited States: Time-Dependent Density Functional Theory and Density Functional Theory Based Multireference Configuration Interaction. *J. Chem. Phys.* **2008**, *128*, 104103/1–14.
- (31) Kleinschmidt, M.; Tatchen, J.; Marian, C. M. Spin–Orbit Coupling of DFT/MRCI Wavefunctions: Method, Test Calculations, and Application to Thiophene. *J. Comput. Chem.* **2002**, *23*, 824–833.
- (32) Kleinschmidt, M.; Marian, C. M. Efficient Generation of Matrix Elements of One-Electron Spin-Orbit Operators. *Chem. Phys.* **2005**, *311*, 71–79.
- (33) Hess, B. A.; Marian, C. M.; Wahlgren, U.; Gropen, O. A Mean-Field Spin–Orbit Method Applicable to Correlated Wavefunctions. *Chem. Phys. Lett.* **1996**, *251*, 365–371.
- (34) AMFI is an atomic spin-orbit integral program written by Schimmelpfennig, B., University of Stockholm, 1996.
- (35) Tatchen, J.; Marian, C. M. On the Performance of Approximate Spin–Orbit Hamiltonians in Light Conjugated Molecules: The Fine-Structure Splitting of HC_6H^+ , NC_5H^+ , and NC_4N^+ . *Chem. Phys. Lett.* **1999**, *313*, 351–357.
- (36) Danovich, D.; Marian, C. M.; Neuheuser, T.; Peyerimhoff, S. D.; Shaik, S. Spin–Orbit Coupling Patterns Induced by Twist and Pyramidalization Modes in C_2H_4 : A Quantitative Study and a Qualitative Analysis. *J. Phys. Chem. A* **1998**, *102*, 5923–5936.
- (37) Etinski, M.; Tatchen, J.; Marian, C. M. Time-Dependent Approaches for the Calculation of Intersystem Crossing Rates. *J. Chem. Phys.* **2011**, *134*, 154105–1–154105–9.
- (38) Duschinsky, F. The Importance of the Electron Spectrum in Multi Atomic Molecules Concerning the Franck-Condon Principle. *Acta Physicochim.* **1937**, *7*, 551–566.
- (39) Marian, C. M. Spin–Orbit Coupling and Intersystem Crossing in Molecules. *WIREs Comput. Mol. Sci.* **2012**, *2*, 187–203.
- (40) Langhoff, S. R.; Kern, C. W. Molecular Fine Structure. In *Modern Theoretical Chemistry*, ed. by H. F. Schaefer III; Plenum: New York, 1977; Vol. 4, pp 381–437.
- (41) Kleinschmidt, M.; Tatchen, J.; Marian, C. M. SpockCI: A Multireference Spin–Orbit Configuration Interaction Method for Large Molecules. *J. Chem. Phys.* **2006**, *124*, 124101–1–124101–17.
- (42) Klamt, A.; Schüürmann, G. COSMO - A New Approach to Dielectric Screening in Solvents with Explicit Expressions for the Screening Energy and its Gradient. *J. Chem. Soc., Perkin Trans.* **1993**, *2*, 799–805.
- (43) Schäfer, A.; Klamt, A.; Sattel, D.; Lohrenz, J.; Eckert, F. COSMO Implementation in TURBOMOLE: Extension of an Efficient Quantum Chemical Code towards Liquid Systems. *Phys. Chem. Chem. Phys.* **2000**, *2*, 2187–2193.
- (44) Mertz, E. L.; Krishtalik, L. I. Low Dielectric Response in Enzyme Active Site. *Proc. Natl. Acad. Sci. U.S.A.* **2000**, *97*, 2081–2086.
- (45) Siegbahn, P. E.; Himo, F. The Quantum Chemical Cluster Approach for Modeling Enzyme Reactions. *WIREs Comput. Mol. Sci.* **2011**, *1*, 323–336.
- (46) Sung, M.; Moore, T. A.; Song, P.-S. Molecular Luminescence Studies of Flavines. I. Excited States of Flavines. *J. Am. Chem. Soc.* **1972**, *94*, 1730–1740.
- (47) El-Sayed, M. A. The Triplet State: Its Radiative and Nonradiative Properties. *Acc. Chem. Res.* **1968**, *1*, 8–16.
- (48) Englman, R.; Jortner, J. Energy Gap Law for Radiationless Transitions in Large Molecules. *Mol. Phys.* **1970**, *18*, 145–164.
- (49) Maciejewski, A.; Steer, R. P. The Photophysics, Physical Photochemistry, and Related Spectroscopy of Thiocarbonyls. *Chem. Rev.* **1993**, *93*, 67–98.